ELSEVIER

Chemical Physics 195 (1995) 339–350

Chemical Physics

Low-frequency motions in an alkali phosphate glass studied by ^{7}Li and ^{31}P NMR

B. Rufflé, S. Beaufils, J. Gallier

Groupe Matière Condensée et Matériaux, URA 804–Université de Rennes I, Campus de Beaulieu, F-35042 Rennes Cedex, France

Received 27 December 1994

Abstract

A ^{31}P and ^{7}Li NMR study of the phosphate glass $Na_{0.5}Li_{0.5}PO_3$ leads to the following dynamical picture. Below T_g, only the Li ions diffuse slowly in the glass structure. This motion seems unaffected by the glass transition and presents a linear frequency dependent spectral density in the two probed frequency ranges. This behaviour, classical in glasses, could be explained by soft potential modes occurring with a high density in this disordered material. Above T_g, the phosphate units of the polymer chains begin to move isotropically giving rise to the so-called secondary relaxation in glasses while the primary or structural relaxation is only effective on the NMR parameters near 600 K, well above T_g.

1. Introduction

An ionically conducting glass provides at least two challenges in the field of relaxation in complex systems. On the one hand, the dynamics of the glassy network lead us to the problem of the liquid–glass transition which is currently of great interest [1]. On the other hand, the mechanism of ionic transport in vitreous materials is still an open question [2]. Nowadays, it is believed that in order to contribute to the understanding of these two topics, several different techniques should be used, trying to cover the widest frequency/timescale range as possible.

In this framework, we have undertaken to study the dynamical behaviour of an alkali metaphosphate glass by means of mechanical, calorimetric and dielectric spectroscopies, nuclear magnetic resonance and neutron and light scattering. The system under study ($Na_{0.5}Li_{0.5}PO_3$) is an inorganic polymer based on the phosphorus oxygen backbone. The basic structural unit is the PO_4 group linked with two neighbouring tetrahedrons forming an infinite twisted chain [3]. The lithium and sodium cations, linked with non-bridging oxygens of the chain, are probably randomly distributed in the glass. This eutectic composition is a poor ionic conductor [4] and occupies an interesting position in known glassforming systems between 'strong' and 'fragile' liquid in the Angell's classification [5].

In this paper, we focus on the results obtained by applying ^{31}P and ^{7}Li NMR on this glass former $Na_{0.5}Li_{0.5}PO_3$. Above the calorimetric glass transition temperature T_g, the study of the phosphorus nucleus provides access to a low-frequency motion of the phosphate chains (timescale 10^{-4}–10^{-6} s)

0301-0104/95/$09.50
SSDI 0301-0104(95)00065-8

whereas below T_g, the study of the lithium nucleus probes the dynamics of the ionic diffusion in the amorphous structure.

2. Material and methods

$Na_{0.5}Li_{0.5}PO_3$ was prepared by mixing the appropriate amount of carbonates Li_2CO_3 and Na_2CO_3 with $(NH_4)_2HPO_4$ of analytical grade. They were melted about 15 min at 700 K in order to expel CO_2, NH_3 and H_2O, then cast on a plate as small transparent balls [6]. As all water was not removed from the glass, the phosphate chain length was not infinite. In fact, our NMR measurements were made on samples with a mean chain length of about twelve tetrahedra PO_4. In this case, the glass transition temperature T_g, determined by conventional differential scanning calorimetry, was lowered to 485 K instead of 515 K for an infinite chain length sample. This technique has also shown that the residual water remained in the structure up to 660 K.

The NMR study was mainly carried out on a Bruker SXP 4-100 pulse spectrometer at various resonance frequencies between 12 and 36 MHz. The temperature was varied and regulated with a standard Bruker system between 300 and 600 K. Few measurements were also made around 150 K. The temperature was constant to better than 0.2 K and its gradient in the sample lower than 2 K. Above about 550 K, the compound was running and the balls merging but the sample was keeping its transparency and the NMR parameters had unchanged values when afterwards the temperature was lowered. The spin–lattice relaxation time T_1 was measured with the $180°-\tau-90°$ pulse sequence but for long T_1, greater than about 5 s, it was obtained by the saturation 90° pulses sequence. In the intermediate T_1 range, we have verified that the same value was given by the two methods. The spin–lattice relaxation time in the rotating frame $T_{1\rho}$ was determined with the spin-locking method for different values of the spin-lock field B_1 – or spin-lock frequency ν_1. The second moment of the resonance line M_2 was derived from the free induction decay (FID) by a least-squares fit with a Gaussian function which describes appropriately the resonance line:

$$G(t) = G(0)\exp\left[-M_2(t^2/2)\right]. \quad (1)$$

Above 500 K for the ^{7}Li spins and 570 K for the ^{31}P spins, the interactions were strongly averaged by the motions so M_2 was nearly zero. The Hahn spin echo $90°-\tau-180°$ pulse sequence was then used to determine the true spin–spin relaxation time T_2 of the spins. Hence, three NMR parameters T_1, $T_{1\rho}$, T_2 or M_2 were measured for each ^{7}Li and ^{31}P nucleus. Finally, we have also made static and MAS spectra on both spins at room temperature on a MSL 300 MHz Bruker spectrometer.

In the case of ^{23}Na, no signal was observed on our spectrometer below 550 K. At the highest temperature studied (600 K), only the central line was seen, the satellite ones were still too much broadened.

3. Experimental results

3.1. ^{31}P nucleus

The resonance line second moment versus temperature is plotted in Fig. 1. A plateau is observed between room temperature up to about 420 K. Its value is frequency dependent: 0.028, 0.014 and 0.012 mT^2 at respectively 36.4, 18 and 12 MHz. Above 420 K, M_2 decreases and becomes zero near 580 K. The M_2 values depend linearly on the square of the Larmor frequency ν_I as it is shown in Fig. 2. The frequency dependent part of the second moment is the chemical shift contribution (CSA), while the dipolar one is given by the zero frequency crossing.

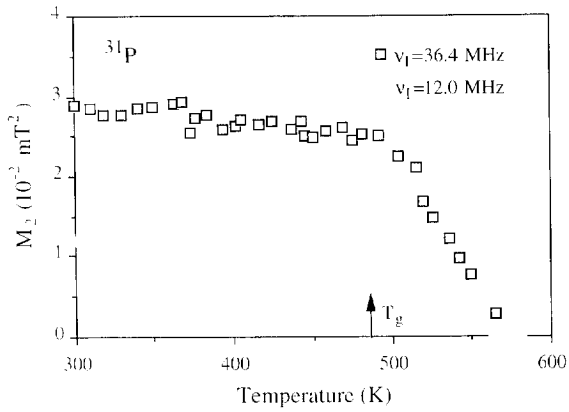

Fig. 1. ^{31}P resonance line second moment versus temperature at two frequencies ν_I = 12 and 36.4 MHz.

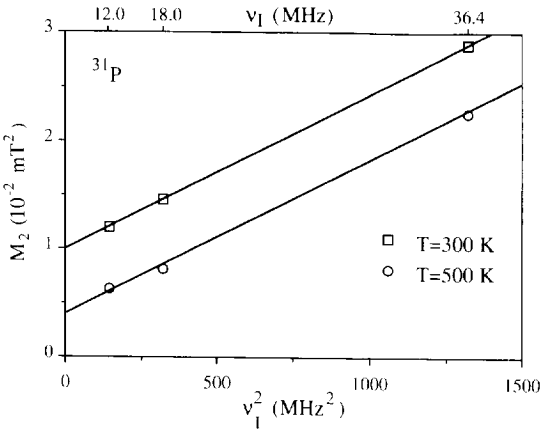

Fig. 2. Frequency dependence of the ^{31}P resonance line second moment at two temperatures $T = 300$ and 500 K. The full lines have the same slope: 1.4×10^{-17} mT^2 s^{-2}.

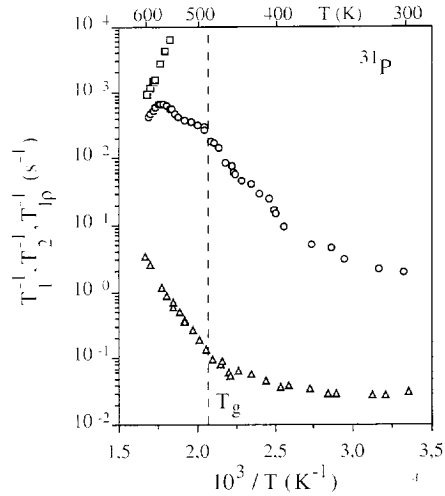

Fig. 3. ^{31}P NMR spin–lattice T_1^{-1} (triangles), spin–spin T_2^{-1} (squares) and spin–lattice in the rotating frame $T_{1\rho}^{-1}$ (circles, $\nu_1 = 10.4$ kHz) relaxation rates as a function of reciprocal temperature. Open symbols: $\nu_I = 35$ MHz, solid symbols: $\nu_I = 18$ MHz.

At 300 and 500 K, the first contribution is unchanged, equal to 1.4×10^{-17} ν_I^2 (mT^2 s^{-2}), while the second has decreased from 0.010 to 0.004 mT^2.

The temperature dependences of the relaxation rates T_1^{-1}, $T_{1\rho}^{-1}$, T_2^{-1} are plotted in Fig. 3. In the limit of accuracy, exponential recovery of the magnetization is followed in the whole temperature range for all the relaxation times. T_1^{-1} presents a very small thermal dependence below 450 K and increases steadily with temperature above 500 K with increasing slope. Besides, at any temperature, the relaxation rate depends weakly on the Larmor frequency. It is not easy to precise the law, owing to the limited accuracy of our measurements and above all to the small frequency range studied. A linear law between the relaxation time T_1 and the Larmor frequency ν_I seems however the more appropriate.

$T_{1\rho}^{-1}$ shows a similar behaviour: at low temperatures, it is weakly temperature dependent; above about 400 K, it becomes governed by two activated processes, which give two maxima of the spin–lattice relaxation rate in the rotating frame near 505 and 565 K. The low temperature maximum is not Larmor frequency dependent and equal to 330 s^{-1} for the spin-lock frequency $\nu_1 = 10.4$ kHz. The high tem-

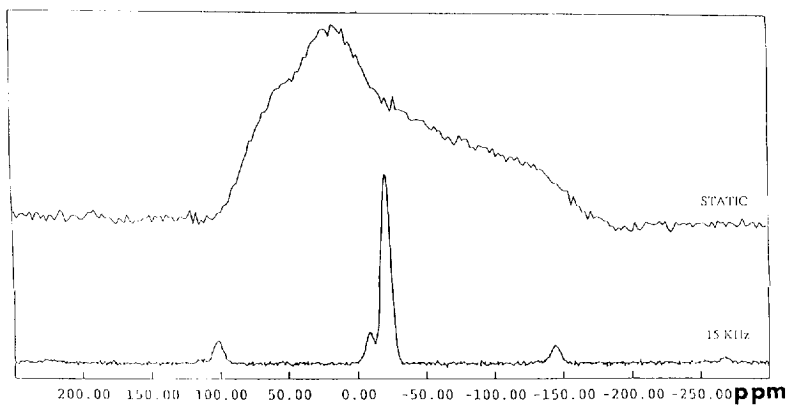

Fig. 4. ^{31}P NMR MAS spectra at $\nu_I = 121.5$ MHz at room temperature for different spinning rates.

perature maximum is much greater at 35 MHz than at 18 MHz; of course, it is due to the CSA contribution already observed on the second moment while the first maximum is of dipolar origin. Below 500 K, the temperature and frequency dependences of the spin–lattice relaxation in the rotating frame can be summarized by the following expression

$$^{31}P T_{1\rho}^{-1} = 2.0 \times 10^{12} e^{-6600/T} \nu_1^{-1} \quad (2)$$

in the ν_1 range (2–20 kHz) of our study.

The spin–spin relaxation time $^{31}P T_2$ is measurable only above 550 K, when the resonance line becomes Lorentzian; as the second moment, it is also Larmor frequency dependent. In the limited temperature range 550–600 K, it is given by

$$^{31}P T_2^{-1} = 2.6 \times 10^{-8} e^{14000/T} \quad (3)$$

at 18 MHz and two times higher at 35 MHz.

The MAS spectrum observed at 121.5 MHz at room temperature on this sample shows two lines (Fig. 4) of respectively weight 0.83 and 0.17; their chemical shift tensor have as main values: isotropic part: $\sigma_{iso} = -21.3$ ppm; chemical shift anisotropy (CSA): $\delta_\sigma = -141.2$ ppm; asymmetry parameter: $\eta_\sigma = 0.5$ for the more populated site, while for the other site, we have: $\sigma_{iso} = -8.9$ ppm; $\delta_\sigma = -116.3$ ppm; $\eta_\sigma = 0.8$. We can simply attribute these two sites to ^{31}P nuclei located respectively inside the phosphate chains and at the ends of the chains. A value for the mean chain length, equal to twelve phosphate units, is thus derived. This attribution is confirmed by an NMR measurement of the density of hydrogens in the sample. Indeed the phosphate chains end by OH groups so that the number of hydrogens is related to this mean chain length. A ratio equal to 6 between the phosphorus and hydrogen densities is found for this sample, in agreement with the attribution of the MAS spectrum.

3.2. ^7Li nucleus

The second moment of the resonance line versus temperature is plotted in Fig. 5. A plateau is observed below 400 K; its value, about 0.0085 mT^2, is not frequency dependent. Above 400 K, M_2 decreases and becomes zero near 510 K. Between about T_g and 530 K, the ^7Li signal amplitude increases sharply with temperature which disagrees with the Curie law observed outside this temperature range. Corrected for the Boltzmann temperature factor, the signal below T_g is only 40% of its high temperature value at 530 K. This amplitude variation is easily understood. At low temperatures, only the central resonance line of the $\frac{3}{2}$ spin ^7Li is seen; the two satellite ones are shifted too far away and broadened by the quadrupolar first-order interaction. This results in an inobservable signal for the satellites as lost in the dead time of the spectrometer. At high temperatures, the Li atomic motion averages strongly the dipolar and quadrupolar interactions so the satellite lines contribute more and more to the observed FID. At 530 K, the broadening and shift are enough reduced so that the whole signal from ^7Li spins becomes observable.

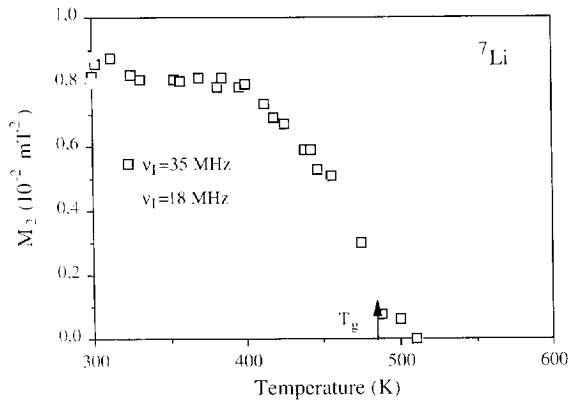

Fig. 5. ^7Li resonance line second moment versus temperature at two frequencies $\nu_I = 18$ and 35 MHz.

The $^{7Li}T_1^{-1}$, $^{7Li}T_{1\rho}^{-1}$ and $^{7Li}T_2^{-1}$ relaxation rates are shown in Fig. 6. Magnetization recovery is well exponential for T_1 but not for $T_{1\rho}$ and in this figure, the $T_{1\rho}$ values are those measured when the magnetization has reached 1/e of its initial value. The spin–lattice relaxation $^{7Li}T_1^{-1}$ increases continuously when the temperature raises with an increasing slope. Above 450 K, the slope is constant and the spin–lattice relaxation rate given by

$$^{7Li}T_1^{-1} = 9.3 \times 10^{13} e^{-6600/T} \nu_I^{-1}, \quad (4)$$

showing the same linear Larmor frequency dependence as already seen on $^{31}P T_1$ and the same activation energy value (6600 K) as for $^{31}P T_{1\rho}$. At lower

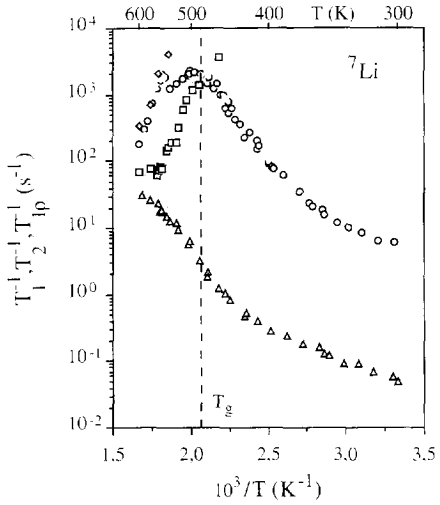

Fig. 6. ^{7}Li NMR spin–lattice T_1^{-1} (triangles), spin–spin T_2^{-1} (central resonance line: squares, satellites lines: diamonds) and spin–lattice in the rotating frame $T_{1\rho}^{-1}$ (circles, $\nu_1 = 10.4$ kHz) relaxation rates as a function of reciprocal temperature. Open symbols: $\nu_I = 35$ MHz, solid symbols: $\nu_I = 18$ MHz.

temperatures, both the temperature and frequency dependences become much weaker, approaching

$$^{7\text{Li}}T_1^{-1} = 17.5/T^{1/2}\nu_I^{-1/2} \quad (5)$$

around 150 K.

The spin–spin relaxation of the central resonance line follows successively two thermal dependences in the small temperature range where it is measured. Just below 500 K, we can write

$$^{7\text{Li}}T_{2c}^{-1} = 2 \times 10^{-3} e^{6600/T}, \quad (6a)$$

while above 500 K, the expression

$$^{7\text{Li}}T_{2c}^{-1} = 7.3 \times 10^{-10} e^{14000/T} \quad (6b)$$

describes the relaxation. The two different activation energies already observed in the ^{31}P study are thus found again. At the highest temperatures, $^{7\text{Li}}T_{2c}^{-1}$ becomes governed by the spin–lattice relaxation and so does not continue to decrease and becomes Larmor frequency dependent. Furthermore, above 550 K, the spin–spin relaxation of the satellite lines can also be measured yielding the same activation energy (14000 K) as the central component in this temperature range, according to

$$^{7\text{Li}}T_{2s}^{-1} = 2.5 \times 10^{-8} e^{14000/T}. \quad (7)$$

The spin–lattice relaxation in the rotating frame $^{7\text{Li}}T_{1\rho}^{-1}$ shows only one maximum at 500 K, independent of the Larmor frequency. Between 400 and 500 K, $^{7\text{Li}}T_{1\rho}^{-1}$ is well described by the following relation:

$$^{7\text{Li}}T_{1\rho}^{-1} = 1.5 \times 10^{13} e^{-6600/T}\nu_1^{-1}. \quad (8)$$

We find again the linear dependence versus the spin-lock frequency ν_1 and the activation energy (6600 K) characteristic of this temperature range. Remember that in this temperature range below 500 K, the measured $^{7\text{Li}}T_{1\rho}$ is only relative to the central resonance line. As said above, at higher temperatures, the satellite lines contribute more and more to the ^{7}Li signal, so that the $^{7\text{Li}}T_{1\rho}$ values become more and more affected by the satellite contribution. This explains the complex thermal behaviour above 500 K: at temperatures just above the $T_{1\rho}^{-1}$ maximum, $^{7\text{Li}}T_{1\rho}^{-1}$ decreases more slowly than expected, then increases and above 550 K is simply given by

$$^{7\text{Li}}T_{1\rho}^{-1} = 0.6\ ^{7\text{Li}}T_{2s}^{-1}. \quad (9)$$

This last relation has a particular meaning: it can only be obtained if two conditions are simultaneously satisfied. Firstly, the fast motional narrowing limit for the motion governing the relaxation is obtained, giving the same spectral density value at ω_1 and at zero frequency. Secondly, the whole ^{7}Li signal relaxes with the same relaxation rate, this common spin–lattice relaxation rate being given by the weighted average of the relaxation rates of the two components of the signal. As the satellite lines relax much faster than the central line ($T_{2s}^{-1} = 35\ T_{2c}^{-1}$) and contribute with sixty percent to the whole signal, it results the factor 0.6 in (9). This common relaxation occurs simultaneously with the appearance of the exponential character of the magnetization recovery of the spin–lattice measurements in the rotating frame. The non-exponentiality observed at lower temperatures is thus shown to be of quadrupolar origin since it disappears with the quadrupolar interaction itself.

The ^{7}Li static and MAS spectra observed at room temperature and 116.6 MHz are shown in Fig. 7. The main values of the quadrupolar coupling are derived: the quadrupolar frequency ν_Q is about 46 kHz and the asymmetry parameter $\eta_Q = 0.8$.

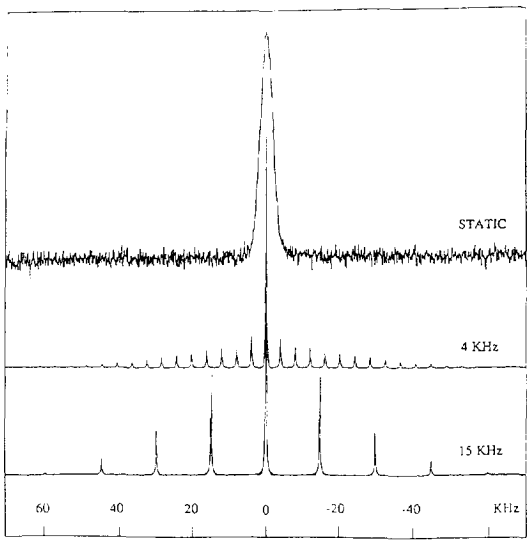

Fig. 7. ^{7}Li NMR MAS spectra at $\nu_I = 116.6$ MHz at room temperature for different spinning rates.

We have also made this NMR study on another sample, prepared differently [7] in order to eliminate water during the synthesis giving a much longer chain length (ratio N_P/N_H about 100). Preliminary measurements have only shown some minor changes in the results. Thus the ^{31}P $M_2(T)$ curve is shifted by about 30 K towards the high temperatures, in agreement with the increase of the glass transition temperature T_g. For ^{7}Li spin, major experimental features can be accounted for by a smaller positive temperature shift of 13 K. Consequently we can infer that the low frequency motional behaviour in this glass, as probed by NMR, is mostly influenced by the local structure. The long-range characteristics of the glass as the chain length do play a minor role.

4. Discussion

This study clearly shows the presence of two distinct motions in this glassy system. The first one, as revealed by the spin–lattice relaxation of both spins (see (2), (4) and (8)) and also by the spin–spin relaxation of ^{7}Li nuclei (6a) is the predominant mechanism below 500 K. It narrows too the ^{7}Li central resonance line. It is obviously the diffusion of the lithium ions in the material. This process is activated, the associated energy, given by the slope of the thermal dependence of the considered NMR parameter, amounts to 6600 K. This value is also found from the ^{7}Li second moment versus temperature curve (Fig. 1). All the measured parameters give the 6600 K energy value for the Li diffusion process.

The second motion is the predominant mechanism above 550 K. It averages completly the ^{31}P resonance line second moment and obviously involves the phosphate chains. This chain motion raises the high temperature maximum of the ^{31}P spin–lattice relaxation rate $T_{1\rho}^{-1}$. It also contributes to the ^{31}P and ^{7}Li spin–spin relaxations. All these parameters lead to a common value of the activation energy for this process, about 14000 K as found in the expressions (3), (6b), and (7) and as given too by the M_2 decrease.

Beyond the knowledge of the activation energy values, which describe the thermal dependence of the two motions in their respective limited temperature range, we shall try to characterize better these motions. In particular we shall attempt to precise the correlation time of each motion and to determine if they are, or not, distributed over any time scale. We shall also discuss the weak frequency dependence of the spin–lattice relaxations, observed on both nuclei.

4.1. Chain motion

The couplings modulated by this motion are, for the ^{31}P spins, the dipolar spin–spin term and the chemical shift anisotropy. The CSA is more specific of the chain motion, while the dipolar one is also dependent of the Li diffusion. The difference between relaxation rates measured at two Larmor frequencies allows to eliminate the dipolar contribution leaving only the CSA one. This difference is then given by [8,9]

$$\left(\Delta^{31}P T_2^{-1}\right) = \Delta C_\sigma \; J^{\text{chain}}(0), \tag{10a}$$

$$\left(\Delta^{31}P T_{1\rho}^{-1}\right) = \Delta C_\sigma \; J^{\text{chain}}(\omega_1), \tag{10b}$$

where

$$\Delta C_\sigma = \frac{4\pi^2}{10}\delta_\sigma^2\left(\nu_{I1}^2 - \nu_{I2}^2\right)\left(1 + \frac{\eta_\sigma^2}{3}\right). \tag{11}$$

In (10), $J^{\text{chain}}(\omega)$ is the spectral density of the chain motion. With $\nu_{I1} = 35$ MHz, $\nu_{I2} = 18$ MHz, $\delta_\sigma =$

137 ppm, $\eta_\sigma = 0.55$ being the mean values of CSA and asymmetry parameter over the two sites deduced from the MAS spectra, it follows $\Delta C_\sigma = 0.73 \times 10^8$ s^{-2}. In Fig. 8 are plotted $(\Delta^{31}P T_2^{-1})$ and $(\Delta^{31}P T_{1\rho}^{-1})$ experimental values together with the calculated ones using the simplest spectral density $J^{chain}(\omega) = \tau_{chain}/(1 + \omega^2\tau_{chain}^2)$. The correlation time τ_{chain} has the 14000 K thermal energy. Its preexponential factor, the only free parameter, is thus derived giving:

$$\tau_{chain} = 3.2 \times 10^{-16} e^{14000/T}. \quad (12)$$

The agreement is rather good owing to the limited accuracy of experimental values obtained as difference between measured relaxation rates. Nevertheless, it shows that the chain motion observed via the CSA coupling behaves as having a single correlation time. Indeed, in the case of a distributed correlation time, the slope measured on the $T_{1\rho}^{-1}$ low temperature side is lesser than the T_2^{-1} one, which disagrees with the experience as shown in Fig. 8. In Fig. 9 are plotted τ_{chain} given by (12) and the characteristic time τ_s of the viscous flow obtained from viscosity measurements on this glass [10]. It seems that above 600 K, the time scales of these two processes become close to each other while below that temperature they are strongly decoupled, giving rise to a primary slow relaxation and to a secondary one. Such motional decoupling has been recently reported on another phosphate glass [11]. Though above 550

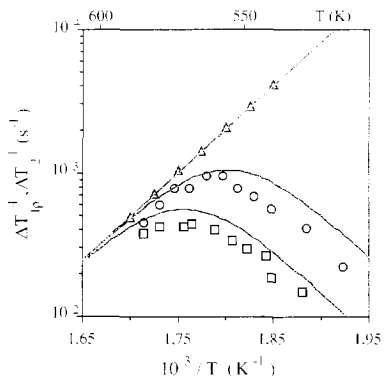

Fig. 8. $^{31}P\Delta T_{1\rho}^{-1}$ (squares: $\nu_1 = 10.4$ kHz, circles: $\nu_1 = 5.5$ kHz) and $^{31}P\Delta T_2^{-1}$ (triangles) experimental values obtained by difference between measured relaxation rates at 35 and 18 MHz leaving only the CSA contribution to the relaxation. Lines are calculated relaxation rates given by (10), (11) and (12) with a Lorentzian chain motion spectral density.

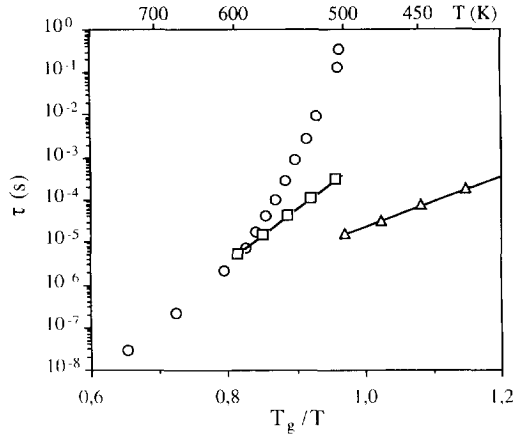

Fig. 9. Correlation times of the chain motion (squares) and of the lithium diffusion (triangles) versus T_g/T as probed by these NMR experiments; correlation time obtained from viscosity measurements [10] (circles).

K, the glass runs in the sample tube and becomes a highly viscous liquid, this primary motion takes only a negligible part in the ^{31}P relaxation because firstly its motional frequency is too small to be observed in this NMR study and secondly, the CSA coupling is above all sensitive to the deformations and reorientations of the PO_4 units forming the chains.

The chain motion governs the relaxations of both spins at high temperature, hence the ^7Li spin–spin relaxation as well. Both the central transition and the satellite ones present the common temperature dependence with a 14000 K activation energy (cf. expressions (6b) and (7)) of their spin–spin relaxation rate. These expressions can be rewritten with τ_{chain} given by (12)

$$^{7Li}T_{2c}^{-1} = C_D^{chain}\tau_{chain}, \quad \text{with } C_D^{chain} = 4.4 \times 10^6 \text{ s}^{-2}, \quad (13a)$$

$$^{7Li}T_{2s}^{-1} = C_Q^{chain}\tau_{chain}, \quad \text{with } C_Q^{chain} = 1.5 \times 10^8 \text{ s}^{-2}. \quad (13b)$$

The prefactor C_D^{chain} in (13a) is expected to be the second moment not still averaged by the Li motion when the chain motion becomes more efficient than the Li diffusion to relax the Li spins. This change of the relaxation process occurs at 500 K. Indeed, the second moment amounts experimentally to 5.4×10^6 s^{-2} at 500 K, a value actually close to C_D^{chain}. The

prefactor C_Q^{chain} in (13b) is too large to be of dipolar origin. It is of course due to the first order quadrupolar interaction which splits and broadens the satellite lines. Its value gives the mean quadrupolar coupling $\nu_Q^{chain} = 3.9$ kHz still present at 500 K [8]. This value is much smaller than the $\nu_Q = 46$ kHz inferred from the ^{7}Li MAS spectra. This is expected since 46 kHz corresponds to the quadrupolar interaction characteristic of the rigid structure present at room temperature, while ν_Q^{chain} observed at 500 K measures the remaining interaction left by the Li atomic translational motion.

4.2. Li atomic diffusion

It is the main source of relaxation for both spins below 500 K. It seems unaffected by the glass transition as no change in Li activation energy occurs around T_g on any observable parameter. Let us first precise the correlation time best given by the $^{7Li}T_2$ spin–spin relaxation since in the high frequency limit ($\omega_l \tau_{Li} \gg 1$), T_2 depends only on the $J^{Li}(0)$ lithium motion spectral density. Below 500 K, the central transition alone is observed and its broadening is almost completely dipolar, the quadrupolar second-order contribution, estimated to about 60 Hz [8], being much smaller than the 4.0 kHz linewidth (Fig. 7). The dipolar interaction consists of couplings between ^{7}Li spins and between ^{7}Li and other spin species (^{6}Li, ^{31}P, ^{23}Na). An estimation of these different contributions to the central resonance line second moment is given in the Appendix. It allows to calculate the whole ^{7}Li second moment (0.0089 mT^2) which compares well with the experimental value at 300 K (0.0085 mT^2) and to derive τ_{Li}. The spin–spin relaxation rate of dipolar origin is indeed related to the second moment M_2^{Li}:

$$^{7Li}T_{2c}^{-1} = M_2^{Li}\tau_{Li}. \tag{14}$$

If we take into account that the correlation time is two times smaller when both spins move i.e. for homonuclear interactions, one obtains

$$^{7Li}T_{2c}^{-1} = C_D^{Li}\tau_{Li} = 6.3 \times 10^7\ \tau_{Li}. \tag{15}$$

By comparison with the experimental T_{2c}^{-1} value expressed by (6a), τ_{Li} is then deduced as

$$\tau_{Li} = 3.2 \times 10^{-11} e^{6600/T}. \tag{16}$$

τ_{Li} given by (16) is also plotted in Fig. 9. Its timescale is well separated from the chain motion one. Its activation energy is notably smaller than the energy of the dc conductivity measured on this phosphate glass amounting to 15000 K [4]. Such disagreement between ^{7}Li NMR and conductivity results is commonly observed on amorphous materials [12–15]. It points out that the two measurements, though involving the same ions, differ markedly. NMR couplings are short-range interactions. The ionic diffusion process occurs through individual jumps between two neighbouring sites. The jumping frequency depends mainly on the local environment around each equilibrium sites and the barrier height to jump is the thermal energy. On the other hand, the dc conductivity is a ionic transport on a long-range scale. In this displacement, the whole structure must undergo some degree of reorganization in order to accommodate the ion transit [16]. Therefore, the thermal energy required in this process must be close to a 'structural' relaxation energy. Indeed, the 15000 K value found for dc conductivity is very close to the 14000 K one followed by the chain motion. This suggests that the deformations and reorientations of the phosphate groups are involved in the long-range displacement of the Li ions. However, as these two energies are observed respectively below and above T_g, this conclusion to be valid supposes that the chain motion keeps the same energy through the glass transition. Measurements of this structural process below T_g should confirm this result.

The ^{31}P spin–lattice relaxation in the rotating frame comes from the heteronuclear dipolar interaction between the ^{31}P and ^{7}Li spins. A 0.005 mT^2 decrease of the ^{31}P resonance line second moment takes place below 500 K (Fig. 1) where the only efficient motion comes from Li spins. The ^{31}P spin–lattice relaxation rate in the rotating frame is then inferred for a dipolar interaction:

$$^{31P}T_{1\rho}^{-1} = C_D^{P\text{-}Li} J^{Li}(2\omega_1) = 5.8 \times 10^7\ J^{Li}(2\omega_1). \tag{17}$$

If the maximum of the spectral density verifies as usually $J_{max}^{Li}(2\omega_1) = (2\omega_1)^{-1}$, then a ^{31}P maximum relaxation rate of 215 s^{-1} at 505 K is expected for $\nu_1 = 10.4$ kHz. The experimental value is about 330 s^{-1} close to the expected value and occurs at 505 K

(Fig. 3). On the other hand, the ^{7}Li spin–lattice relaxation rate in the rotating frame is due to dipolar and quadrupolar interactions. The dipolar contribution is similarly given by

$$^{7,i}T_{1\rho_D}^{-1} = C_D^{Li} J^{Li}(2\omega_1) = 6.3 \times 10^7 \; J^{Li}(2\omega_1). \tag{18}$$

This predicts a 470 s^{-1} maximum at 505 K for this contribution. The ^{7}Li experimental value is rather 2300 s^{-1} at 500 K, nearly 5 times higher (Fig. 6). Therefore, the dipolar interaction is not the main contribution to the spin–lattice relaxation rate $^{7Li}T_{1\rho}^{-1}$. The first-order quadrupolar interaction which does not participate to the broadening of the central resonance line, does however contribute to its spin–lattice relaxation since it modifies the populations of the $\pm\frac{1}{2}$ spin states. This quadrupolar contribution can be estimated from the observed $^{7Li}T_{1\rho}^{-1}$ maximum value to 2.4×10^8 s^{-2}. There is, to our knowledge, no theoretical expression giving the quadrupolar relaxation in the rotating frame of a spin $\frac{3}{2}$. But it is well-known for the spin–lattice relaxation in the Zeeman field when a rapid spin diffusion gives a single relaxation rate [17,18]

$$^{7Li}T_{1_Q}^{-1} = C_Q^{Li}\left[\left(J^{Li}(\omega_l) + 4J^{Li}(2\omega_l)\right)\right], \tag{19}$$

with

$$C_Q^{Li} = \frac{4\pi^2}{25}\nu_Q^2\left(1 + \frac{\eta_Q^2}{3}\right)$$

for a powder sample. Since the Li motion takes place in the rigid amorphous structure, the ν_Q value above is the one observed at room temperature on the MAS spectrum (Fig. 7), i.e. 46 kHz giving $C_Q^{Li} = 4.0 \times 10^9$ s^{-2}, one order of magnitude more than the quadrupolar constant derived from the experimental $^{7Li}T_{1\rho}^{-1}$ maximum. Such large discrepancy is not easy to explain, more especially as $^{7Li}T_1^{-1}$ measurements are well in agreement with the above C_Q^{Li} value, as shown below when the spin–lattice relaxation in the Zeeman field will be discussed. Such a large difference has been already reported between T_1 and $T_{1\rho}$ values when the quadrupolar interaction plays the main role [12]. The narrowing of the ^{7}Li central resonance line which leads to T_2 longer than $T_{1\rho}$ above 500 K is a possible argument, unless a theory of the spin–lattice relaxation in the rotating frame by quadrupolar interaction gives us the true explanation.

4.3. Frequency dependence of the spectral density $J^{Li}(\omega_l)$

This dependence is well established by our study. The relaxation rate in the rotating frame $T_{1\rho}^{-1}$ for both spins follows a linear law: $T_{1\rho}^{-1} \propto \omega_1^{-1}$ in the low temperature range below 500 K where the Li motion governs the relaxation. On the contrary, at the highest temperatures, the relaxation rates become no longer frequency dependent as usual when $\omega\tau \rightarrow 0$. What is the physical origin of this weak frequency dependence? Numerous theoretical models [19–28] try to account for the special thermal and frequency behaviours observed in glassy materials and ionic conductors. First we can discard all the models, based on a wide range of correlation times, which lead to a specific relation between frequency and temperature dependences. Indeed they assumed that the time correlation function has a stretched exponential form which origin differs from one model to the other. The stretching of this exponential function gives both the spin–lattice frequency dependence ($\omega^{-(1-\beta)}$) and the ratio between the thermal dependences of the relaxation rate observed respectively on the low temperature side and the high temperature side of the maximum. In this phosphate glass, thermal and frequency behaviours of the spin relaxations are not so related. Besides, this eutectic phosphate glass is a rather poor ionic conductor while these models seem to be appropriate to fast ionic conductors in glassy or crystalline state as well. Furthermore in poor ionic conductors, linear or even sublinear frequency dependence has often been found in a large temperature range with a power law temperature dependence in the low temperature region ($T \leqslant 100$ K) [29]:

$$T_1^{-1} \propto \omega^{-\alpha} T^{\gamma} \quad (0 \leqslant \alpha \leqslant 1, \quad \gamma \sim 1), \tag{20}$$

which becomes of Arrhenius type at higher temperatures:

$$T_1^{-1} \propto \omega^{-\alpha} e^{-E_a/kT}. \tag{21}$$

Ionic diffusion in these compounds is not fast enough to contribute efficiently to the spin relaxation. The mechanism of relaxation currently accepted is a Ra-

man process involving excitations and desexcitations of low energy modes typical of glasses, called TLS modes (two level systems) at low temperatures or soft potential configurations [13,30–34]. These modes are thought to arise from the motion of groups of atoms which can occupy two configurations of nearly equal energy. A wide distribution of barrier heights and asymmetry energies in these asymmetric double well potentials yields the weak frequency dispersion and weak thermal dependence observed at low temperature. At higher temperatures when ionic diffusion is present, relaxation would still originate from these soft modes but coupled with ion jumps giving the activated temperature dependence [14,15,35]. This theory unfortunately does not precise the physical characteristics of these modes and above all does not give simple analytic relations between the microscopic parameters of the model and the coefficients experimentally determined, particularly the frequency power law exponent. This phosphate glass being a poor ionic conductor, it is expected this theoretical scheme is convenient and actually it is. However our study shows that all ^{7}Li and ^{31}P spins contribute to their respective relaxation rates so that the density of spins belonging to low frequency soft modes should be identical to the spin density itself. This result is inconsistent with TLS viewed as defects [12,13,31,33] arising from groups of atoms sited in two configurations separated by a small energy difference. However, other authors have found such high densities of soft modes [32]. Accordingly the true origin of the weak frequency dependence for the $J^{\mathrm{Li}}(\omega)$ spectral density is still questionable.

4.4. Spin–lattice relaxation in the Zeeman field

As described above, T_1^{-1} is dominated for both spins at low temperature by a slow temperature dependence and at high temperature by a thermally activated one. For the ^{7}Li spin–lattice relaxation the activated part has the true energy (6600 K) of the Li motion (4), while for the ^{31}P relaxation rate, it is not so well defined as the slope of the $\ln T_1^{-1}$ versus (T^{-1}) curve increases with temperature, ranging from 6600 K near 500 K up to 9000 K at the highest temperatures. An increasing slope is expected when a second process, more strongly activated, the phosphate chain motion, begins to contribute efficiently to the observed relaxation and adds to the Li motion contribution. The ^{7}Li spins are relaxed mainly via quadrupolar interaction as only such large interaction is able to give so high relaxation rates. The ^{31}P spins are relaxed first from heteronuclear dipolar interaction when Li motion alone is efficient, then secondly from CSA when phosphate chains move i.e. in the highest temperature region. When only the Li motion is present, we can estimate the ratio between the spin–lattice relaxations of the two spins since the same spectral density $J^{\mathrm{Li}}(\omega)$ contribute to the two relaxation rates:

$$^{7\mathrm{Li}}T_1^{-1} = C_{\mathrm{Q}}^{\mathrm{Li}}\left[J^{\mathrm{Li}}(\omega_I) + 4J^{\mathrm{Li}}(2\omega_I)\right], \tag{22a}$$

$$^{31\mathrm{P}}T_1^{-1} = C_{\mathrm{D}}^{\mathrm{P-Li}}\left[0.5J^{\mathrm{Li}}(\omega_I - \omega_S)\right]. \tag{22b}$$

The prefactors $C_{\mathrm{Q}}^{\mathrm{Li}}$ and $C_{\mathrm{D}}^{\mathrm{P-Li}}$ are known and the linear frequency dependence shown by the $J^{\mathrm{Li}}(\omega)$ spectral density is found valid in the MHz range as well as in the kHz range. Thus $(^{7\mathrm{Li}}T_1^{-1}/^{31\mathrm{P}}T_1^{-1}) = 6(C_{\mathrm{Q}}^{\mathrm{Li}}/C_{\mathrm{D}}^{\mathrm{P-Li}})\,[1-(\omega_S/\omega_I)] = 26$. The experimental ratio in the activated part of the relaxation rate curves is 25, in excellent agreement. It decreases near the highest temperature (600 K), as the second process participates enough to the ^{31}P relaxation.

The low temperature mechanism could have a priori two different origins: the soft modes already discussed in the interpretation of the activated process or the relaxation by fixed paramagnetic centers which could be present in the sample. The first mechanism can be discarded, at least for ^{7}Li spins, since the frequency dependence of the low temperature process $(\omega^{-1/2})$ is different from the one followed in the thermally activated part (ω^{-1}) in contradiction with this theory predicting the same frequency exponent in both the temperature regions when the soft modes are involved (compare Eqs. (20) and (21)). Furthermore, the frequency and temperature behaviours at low temperatures observed on the ^{7}Li spin–lattice relaxation $(\propto \omega^{-1/2}T^{1/2})$ is just what is expected from relaxation by fixed paramagnetic impurities [36,37]. The second mechanism could also explain the intermediate thermal behaviour of the ^{7}Li relaxation occurring between the square root temperature dependence below room temperature and the strongly activated process above 450 K. In this intermediate range, Li atomic diffusion is fast enough to overcome the spin diffusion process working at

low temperature. The relaxation should become thermally activated but with an apparent activation energy 25% lower than the true one [38]. This result is experimentally observed: corrected from its low temperature contribution, the ^{7}Li spin–lattice relaxation of this intermediate region between 300 and 450 K presents a slope equal to 4200 K close to the 4900 K expected. On the contrary the ^{31}P relaxation has no such intermediate thermal behaviour since phosphate chains are still frozen in this temperature range and thus spin diffusion is the only efficient process.

5. Conclusion

This NMR study clearly shows that two different low frequency motions are present in this glass in the temperature range around the glass transition. Below T_g only the Li ions diffuse in the structure. Above T_g, a rapid motion of the phosphate chains takes place, whereas the Li motion seems unaffected by the glass transition. The mean correlation frequency for this chain dynamics (10^4 s^{-1}, 30 K above T_g) is much larger than the typical frequencies of the viscous flow or primary relaxation of the glass (~ 1 s^{-1}). So this chain motion observed by NMR is attributed to local reorientations of the phosphate groups giving rise to the so-called secondary relaxation of the glass [11,39–41]. Moreover, this chain motion could govern the dc conductivity. The primary relaxation is only effective at the highest temperatures studied where it narrows completely the ^{31}P resonance line. Activation energy and correlation times have been rather well determined for each motion. Likewise, their respective spectral densities have been derived from the frequency behaviour of their relaxation rates. The Li motion spectral density $J^{\mathrm{Li}}(\omega)$ follows a linear frequency dependence in the two measured frequency ranges: in the megahertz as well as in the kilohertz regions. This behaviour, often found in glassy or disordered materials, is not explained unless to call on soft modes with densities as large as Li nuclei or phosphate units. In other respects, the chain motion spectral density $J^{\mathrm{chain}}(\omega)$, only observable at the highest temperatures in the kilohertz range, follows the usual Lorentzian function typical of a non-distributed correlation time. In order to give more insight into the microscopic details of these motions, a NMR spectral study and dielectric measurements are now under way.

Acknowledgement

We greatly acknowledge C. Bessada and D. Massiot (C.R.P.H.T. 45071 Orléans Cedex, France) for providing ^{31}P and ^{7}Li MAS NMR spectra.

Appendix. Calculation of the dipolar contribution to the second moment of the resonance lines in the rigid structure

The glassy sample is treated as a crystalline powder i.e. the internuclear vectors are assumed isotropically distributed in the space. The internuclear distances r_{ij} and the density of the spin species are provided from the crystalline structures of $LiPO_3$ and $NaPO_3$ [42,43]. All the spins inside a sphere of radius 5 nm around each spin of the crystalline unit cell are taken into account in the lattice sums. Lithium and sodium atoms in the eutectic compound $Na_{0.5}Li_{0.5}PO_3$ are supposed uniformely distributed in the structure with an occupancy probability equal to 0.5 on each cation site.

The dipolar second moment is the sum of the homonuclear $M_{2(I-I)}$ and of the heteronuclear $M_{2(I-S)}$ contributions. The homonuclear one is given for the spin $\frac{1}{2}$ ^{31}P [8]

$$M_{2(I-I)} = M_2^{\mathrm{vv}} = \tfrac{3}{5}\gamma^2\hbar^2 I(I+1) C_I N_I^{-1} \sum_{i=1}^{N_I} \sum_{j\neq i} r_{ij}^{-6}, \tag{23}$$

where γ_I is the gyromagnetic ratio, C_I the natural abundance of the I spins and N_I the number of I spins in the unit cell. The index i labels each I spin of the unit cell, while index j labels any other I spin, in the limit of 5 nm for r_{ij}. For the spin $\frac{3}{2}$ ^{7}Li, this contribution is reduced from the above van Vleck value M_2^{vv} by the factor 0.8 valid when quadrupolar nuclei of the same kind interact [44].

The heteronuclear contribution is always given by [8]

$$M_{2(I-S)} = \tfrac{4}{15}\gamma_S^2\hbar^2 S(S+1) C_S N_I^{-1} \sum_{i,j} r_{ij}^{-6}, \tag{24}$$

Table 1

	$LiPO_3$		$Li_{0.5}Na_{0.5}PO_3$
^{7}Li nucleus			
$M_{2(I-I)}$	0.0122		0.0061
$M_{2(I-S)}$	0.0016		0.0028
M_2	0.0138		0.0089
	$LiPO_3$	$NaPO_3$	$Li_{0.5}Na_{0.5}PO_3$
^{31}P nucleus			
$M_{2(I-I)}$	0.0026	0.0026	0.0026
$M_{2(I-S)}$	0.0068	0.0024	0.0046
M_2	0.0094	0.0050	0.0072

where C_S is the natural abundance of the S spins. The index j labels any S spin. The calculated values in mTesla^2 (mT^2) of $M_{2(I-I)}$ and $M_{2(I-S)}$ are thus derived for the crystalline structures. The respective values in the eutectic composition are then obtained. For the ^{31}P nucleus, they are simply given by the average of the two crystalline values. For the ^{7}Li nucleus, the phosphorus contribution is unchanged whereas the lithium one is simply divided by two from the $LiPO_3$ values and the sodium contribution needs lithium–sodium internuclear distances not given by the above X-ray studies. We have taken the mean lattice sum in the $LiPO_3$ and $NaPO_3$ for this intercationic contribution. The results are summarized in Table 1. The experimental ^{7}Li and ^{31}P dipolar second moments are respectively 0.0085 and 0.010 mT^2, in good agreement with the above calculated value 0.0089 and 0.0072 mT^2.

References

[1] A.J. Dianoux, W. Petry and D. Richter, eds., Proceedings of the International Workshop on Dynamical of Disordered Materials II, Physica A 201 (1993).

[2] O. Kanert and J.M. Spaeth, eds., Proceedings of the International Conference on Defects in Insulating Materials (World Scientific, Singapore, 1993).

[3] B.C. Bunker, G.W. Arnold and J.A. Wilder, J. Non Cryst. Solids 64 (1984) 291.

[4] R. Chen, R. Yang, B. Durand, A. Pradel and M. Ribes, Solid State Ionics 53–56 (1992) 1194.

[5] C.A. Angell and W. Sichina, Ann. NY Acad. Sci. 273 (1976) 53.

[6] E. Gueguen, Ph.D. Thesis, Rennes, France (1994).

[7] R. Wäsche and R. Brückner, Phys. Chem. Glasses 27 (1986) 80.

[8] A. Abragam, The Principles of Nuclear Magnetism (Oxford Univ. Press, London, 1961).

[9] D. Canet and J.B. Robert, NMR Principles and Progress, Vol. 25 (1990).

[10] B. Rufflé, unpublished viscosity data.

[11] E. Rössler and P. Eierman, J. Chem. Phys. 100 (1994) 5237.

[12] E. Göbel, W. Müller-Warmuth and M. Olyschläger, J. Magn. Reson. 36 (1979) 371.

[13] A. Avogadro, F. Tabak, M. Corti and F. Borsa, Phys. Rev. B. 41 (1990) 6137.

[14] G. Balzer-Jöllenbeck, O. Kanert, H. Jain and K.L. Ngai, Phys. Rev. B 39 (1989) 6071.

[15] O. Kanert, J. Steinert, H. Jain and K.L. Ngai, J. Non Cryst. Solids 131–133 (1991) 1001.

[16] S.W. Martin and C.A. Angell, Solid State Ionics 23 (1986) 185.

[17] E.R. Andrew and D.P. Tunstall, Proc. Phys. Soc. 78 (1961) 1.

[18] D. Brinkmann, M. Mali, J. Roos, R. Messer and H. Birli, Phys. Rev. B 26 (1982).

[19] R.G. Palmer, D.L. Stein, E. Abrahams and P.W. Anderson, Phys. Rev. Letters 53 (1984) 958.

[20] W. Schirmacher and A. Schirmer, Solid. State Ionics 28–30 (1988) 134.

[21] K. Funke, Solid State Ionics 28–30 (1988) 100.

[22] K. Funke and R. Hoppe, Solid State Ionics 40–41 (1990) 200.

[23] S.R. Elliot and A.P. Owens, Phys. Rev. B 44 (1991) 47.

[24] S.R. Elliot, J. Phys. (Paris) C 2 (1992) 51.

[25] F. Borsa, D.R. Torgeson, S.W. Martin and K.H. Patel, Phys. Rev. B 46 (1992) 795.

[26] K.L. Ngai, Phys. Rev. B 48 (1993) 13481.

[27] M. Meyer, P. Maass and A. Bunde, Phys. Rev. Lett. 71 (1993) 573.

[28] O. Kanert, R. Küchner, K.L. Ngai and H. Jain, Phys. Rev. B 49 (1994) 76.

[29] K.L. Ngai, J. Phys. (Paris) C 2 (1992) 61.

[30] T.L. Reinecke and K.L. Ngai, Phys. Rev. B 12 (1975) 3476.

[31] M. Rubinstein, H.A. Resing, T.L. Reinecke and K.L. Ngai, Phys. Rev. Lett. 34 (1975) 1444.

[32] J. Szetfel and H. Alloul, J. Non Cryst. Solids 29 (1978) 253.

[33] G. Balzer-Jöllenbeck, O. Kanert, J. Steinert and H. Jain, Solid State Commun. 65 (1988) 303.

[34] S. Estalji, O. Kanert, J. Steinert, H. Jain and K.L. Ngai, Phys. Rev. B 43 (1991) 7481.

[35] K.L. Ngai, J.N. Mundy, H. Jain, O. Kanert and G. Balzer-Jöllenbeck, Phys. Rev. B 39 (1989) 6169.

[36] I.J. Lowe and D. Tse, Phys. Rev. 166 (1968) 279.

[37] L. Shen, Phys. Rev. 172 (1968) 259.

[38] Y. Roinel and J.M. Winter, J. Phys. (Paris) 31 (1970) 351.

[39] D. Kivelson and S.A. Kivelson, J. Chem. Phys. 90 (1989) 4464.

[40] E. Rössler, Phys. Rev. Lett. 69 (1992) 1620.

[41] L. Wu and S.R. Nagel, Phys. Rev. B 46 (1992) 11198.

[42] J.C. Guitel and I. Tordjman, Acta Cryst. B 32 (1976) 2960.

[43] Von K.H. Jost, Acta Cryst. 14 (1961) 844.

[44] K. Kambe and J.F. Ollom, J. Phys. Soc. Japan 11 (1956) 50.